Plant cell wall enzymatic deconstruction: Bridging the gap between micro and nano scales

Yassin Refahi, Aya Zoghlami, Thibaut Viné, Christine Terryn, Gabriel Paës

Bioresource Technology 414 (2024) 131551

Contents lists available at ScienceDirect

Bioresource Technology

journal homepage: www.elsevier.com/locate/biortech

Plant cell wall enzymatic deconstruction: Bridging the gap between micro and nano scales

Yassin Refahi [a,*], Aya Zoghlami [a], Thibaut Viné [a], Christine Terryn [b], Gabriel Paës [a,*]

[a] Université de Reims-Champagne-Ardenne, INRAE, FARE, UMR A 614, Reims 51100, France
[b] Platform of Cellular and Tissular Imaging (PICT), Université de Reims Champagne Ardenne, 51100 Reims, France

HIGHLIGHTS

- A novel computational tool is devised to track and quantify cell wall deconstruction.
- Enzymatic hydrolysis mainly impacts wall volume rather than accessible surface area.
- Pre-hydrolysis compactness measures correlate with volumetric deconstruction rate.
- Enzymatic activity tunes the compactness and volumetric deconstruction correlation.
- Volumetric cell wall deconstruction rate correlates with cellulose conversion rate.

GRAPHICAL ABSTRACT

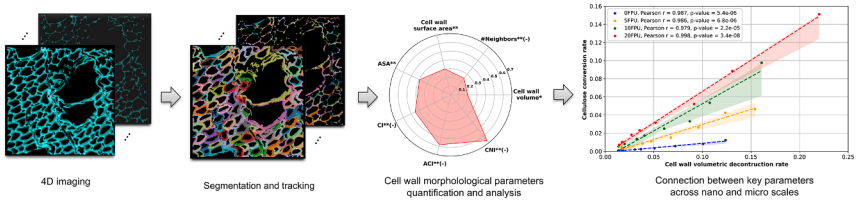

ARTICLE INFO

Keywords:
Lignocellulose
Recalcitrance
4D Imaging
4D cell wall analysis
Morphological parameters
Segmentation
Tracking

ABSTRACT

Understanding lignocellulosic biomass resistance to enzymatic deconstruction is crucial for its sustainable conversion into bioproducts. Despite scientific advances, quantitative morphological analysis of plant deconstruction at cell and tissue scales remains under-explored. In this study, an original pipeline is devised, involving four-dimensional (space + time) fluorescence confocal imaging, and a novel computational tool, to track and quantify deconstruction at cell and tissue scales. By applying this pipeline to poplar wood, dynamics of cellular parameters was computed and cellulose conversion during enzymatic deconstruction was measured. Results showed that enzymatic deconstruction predominantly impacts cell wall volume rather than surface area. Additionally, a negative correlation was observed between pre-hydrolysis compactness measures and volumetric cell wall deconstruction rate, whose strength was modulated by enzymatic activity. Results also revealed a strong positive correlation between average volumetric cell wall deconstruction rate and cellulose conversion rate. These findings link key deconstruction parameters across nano and micro scales.

1. Introduction

The convergence of environmental and economic imperatives due to climate change, increasing global energy demands and unstable oil prices highlights the critical need for a transition from fossil resources towards alternative energy and material sources. Transformation of lignocellulosic biomass into bioproducts offers a renewable eco-friendly carbon–neutral alternative to conventional petroleum derived products

* Corresponding authors.

https://doi.org/10.1016/j.biortech.2024.131551
Received 20 August 2024; Received in revised form 27 September 2024; Accepted 29 September 2024
Available online 5 October 2024

to achieve sustainable development and to ensure the well-being of future generations (Sheldon, 2014; Ashokkumar et al., 2022; Zhang et al., 2023a; Wang et al., 2024). Therefore, transformation of lignocellulosic biomass can be regarded as a critical component of a sustainable bioeconomy to meet humanity's needs while limiting negative impacts on the environment (Antar et al., 2021). The primary building blocks of the plant cell wall are cellulose, hemicelluloses, lignin, and pectins, which are collectively referred to as lignocellulose. Cellulose is composed of linear chains of D-glucose units linked by β-(1,4) glycosidic bonds and is the most abundant biopolymer on Earth (Sorek et al., 2014). Cellulose fibers are enveloped with interweaving hemicelluloses which constitute a group of heterogeneous polysaccharides made of pentose and hexose sugars and other small groups. Lignin, an irregular phenylpropanoid polymer, forms a protective barrier around the polysaccharides (Sorek et al., 2014; Qaseem et al., 2021). Pectins, a complex set of polysaccharides rich in galacturonic acid, contribute to the plant cell wall's porosity, cell–cell adhesion, and plant growth and morphogenesis (Mohnen, 2008). Although different biotechnological processes are used for lignocellulose conversion, a general process consists of pretreatment of lignocellulosic biomass to improve accessibility of cellulose and hemicellulose (Mankar et al., 2021; Haldar and Purkait, 2021) for subsequent enzymatic hydrolysis, called saccharification, to break down the carbohydrates into simpler sugars (predominantly glucose) followed by the fermentation of monosaccharides generated by the saccharification (Binder and Raines, 2010; Khare et al., 2015). Therefore, enzymatic hydrolysis is a crucial step in the conversion process. A major challenge to enhance the release of fermentable sugars during saccharification is to overcome the natural resistance of plant cell wall to deconstruction, called recalcitrance (Himmel et al., 2007). The recalcitrance is a major contributor to the high cost of lignocellulosic biomass derived products. Extensive research has been conducted over the past decades to better understand the recalcitrance and its underlying parameters (McCann and Carpita, 2015). Several recalcitrance markers like lignin content (Santos et al., 2012), cellulose crystallinity (Hall et al., 2010), degree of cellulose polymerization (Meng et al., 2017), and porosity of the cell wall (Herbaut et al., 2018) have been identified. Strikingly, only markers at nano scale have been investigated and quantitative morphological analysis of plant cell wall enzymatic hydrolysis at cell and tissue scales remains under-explored. In the past decade, methods and techniques such as immunolabeling, cellulose staining, and fluorescence imaging have been employed to observe deconstruction of wall polymers and to characterize the dynamics of enzymatic hydrolysis through time-lapse imaging, providing visual evidence of the changes occurring in cells and tissues during the enzymatic deconstruction (Li et al., 2018). Additionally, quantum dot-based fluorescent probes have been utilized to label glycan epitopes, enabling in situ visualization of polysaccharides and lignin distributions in plant cell walls (Yang et al., 2020). Despite these advances, a notable gap in the literature exists regarding micro scale quantitative morphological characteristics contributing to recalcitrance. This lack of understanding is mainly due to the lack of comprehensive quantification of cell and tissue scale structural parameters during enzymatic deconstruction. Acquisition and analysis of time-lapse images during enzymatic hydrolysis is particularly challenging, contributing to the deficiency in understanding.

Several methods have been developed to characterize cellular growth and division of plant and animal tissues (Fernandez et al., 2010; Willis et al., 2016; Guignard et al., 2020; Wolf et al., 2021) which can be seen as the opposite mechanism compared to cell wall deconstruction. These innovative and inspiring methods combine confocal time-lapse live imaging and segmentation and tracking. Nevertheless, these methods are not adapted to address the challenges of plant cell wall deconstruction investigation at cell and tissue scales. To acquire time-lapse images of cell wall deconstruction, the cell walls together with an enzyme cocktail should be imaged at relatively high constant optimal temperature (typically 50°C) for enzymatic reaction while keeping the sample stable and avoiding enzymatic cocktail evaporation during hydrolysis for a substantial number of hours. The deconstruction of the cell wall during hydrolysis compromises the suitability of the pre-existing segmentation and tracking methods. In the early stages of cell wall deconstruction, classical methods require time-consuming laborious manual adjustment of parameters, particularly for large datasets. This can introduce bias, compromising the accuracy, reliability, and objectivity of the results. As hydrolysis advances and cell walls develop holes and cracks, possibly culminating in their complete breakdown, these classical algorithms tend to produce increased segmentation errors.

This study presents an original innovative computational pipeline, named WallTrack, developed to quantify the evolution of cell and tissue scale structural parameters during plant cell wall deconstruction. Poplar is selected as the model plant due to its fast growth rate, ease of in vitro cultivation and vegetative propagation, and extensive distribution. Poplar was the first woody plant, the third angiosperm, after *Arabidopsis* and rice, to have its relatively small genome sequenced (Meng et al., 2017; Müller et al., 2013). Dilute acid pretreatment which is a widely utilized method in industrial processes, is selected for its cost-effectiveness and high efficiency, especially with hardwoods. Dilute acid pretreatment solubilizes hemicelluloses, alters lignin structure, and improves enzyme access to cellulose, thereby enhancing enzymatic hydrolysis (de Oliveira Santos et al., 2018). Using this pipeline, dynamics of key cell wall structural parameters during enzymatic hydrolysis of poplar wood samples were quantified. Additionally, the extent of cellulose conversion, referring to the transformation of cellulose into oligosaccharides and glucose, during the hydrolysis of the poplar samples is assessed. The qualifications are then used to study the relationships among these key structural parameters during deconstruction and to investigate the potential connections between the nano- and micro-scales.

2. Materials and methods

2.1. Sample preparation and compositional analysis

Poplar stem wood (*Populus nigra x deltoides*) was sectioned into fragments measuring 0.4 cm in width, 2 cm in length, and 0.2 cm in thickness using a razor blade. These poplar fragments were subsequently pretreated with 2% dilute sulfuric acid at 170°C for 20 min, following the protocol outlined in (Zoghlami et al., 2019). Transverse sections of xylem from both native and pretreated poplar fragments were then prepared as 40 μm thick slices using a sliding microtome (Stemi 1000, Zeiss, Germany).

For compositional analysis, the samples were ground into particles with a size of 80 μm. The analysis of moisture, ash, lignin, and carbohydrate content in both native and pretreated poplar samples was conducted following the methodology outlined in (Herbaut et al., 2018) (see supplementary material).

2.2. Enzymatic saccharification

Enzymatic hydrolysis experiments on poplar sections were conducted using Cellic CTec2®(Novozymes A/S Bagsværd, Danemark), a commercial enzyme cocktail, chosen for its high hydrolysis efficiency, with a cellulase activity of 195 IU/mL. The reaction mixtures (60 μL of acetate buffer with 0.02% of sodium azide) with the poplar sections were pre-incubated for 30 min at 50°C. The enzymatic hydrolysis was then initiated by adding the enzyme cocktail and followed for 24 h (hrs) at 50°C.

For validation, enzymatic hydrolysis was conducted in two different systems without stirring, replicating the hydrolysis conditions found between a microscope slide and cover slip:

- in the same sealed frame as that used for four-dimensional (space and time), 4D, acquisition under the microscope, installed in a customized incubation chamber;
- mini reactors made of embedded capsules of 6 mm diameter with snap-on integral caps made from polypropylene, highly-resistant to high temperature.

After 24 h of enzymatic hydrolysis, the reaction mixture was analyzed and the concentration of glucose released from enzymatic hydrolysis in the supernatant was determined using a high-performance anionic exchange chromatography (HPAEC-PAD, Dionex) to calculate the cellulose conversion from the pretreated poplar, as previously described (Herbaut et al., 2018). All experiments and analysis were carried out as triplicates.

2.3. Customized incubation chamber for imaging plant cell wall during enzymatic hydrolysis

40 μm-thick cross sections prepared from both native and pretreated poplar samples were incubated in 0.05 M acetate buffer at pH 5 for 30 min prior to mounting in the same medium on a microscope slide covered with a coverslip (0.17 mm thickness) separated by a spacer (Gene frame ®65 μL, Thermo Scientific) to provide a 65 μL sealed chamber containing 60 μL enzyme-buffer solution to avoid the evaporation during the enzymatic hydrolysis. The samples were fixed to the cover slide using a temperature resistant adhesive to avoid the movement of the samples in the reaction mixtures. A stable temperature of 50°C was maintained using an incubator adapted for microscopy (H301-Mini-OKOLab, Italy) to optimize enzymatic activity.

2.4. Fluorescence confocal time-lapse acquisition protocol

To acquire time-lapse confocal images, a laser scanning microscope (Leica TCS SP8, Germany) equipped with 63× oil-immersion objective (numerical aperture = 1.4) was used and z-stacks (with 0.3μm z-step) of both native and pretreated poplar samples were acquired at scan speed of 400 hertz with a resolution of 256 × 256 pixels. A 405 nm laser (4% intensity) was used for imaging cell wall sample autofluorescence by detecting fluorescence emission on the 415–700 nm range using the HyD detector in counting mode. The confocal z-stacks of native and pretreated poplar were taken every 30 min for the first four hours and every one hour until 24 h. The time interval, image resolution and microscope parameters were optimized to avoid sample photo-bleaching. The optimal microscope parameter values were determined as a compromise between suitable acquisition quality for subsequent segmentation and reduced laser exposure.

2.5. Segmentation and tracking

To investigate the cell wall deconstruction at cell and tissue scales, a segmentation and tracking pipeline called WallTrack is devised. WallTrack addresses the challenges associated with autofluorescence intensity reduction generated by the enzymatic deconstruction by initially segmenting the pre-hydrolysis image, at a stage where cell walls are intact and the boundaries between adjacent cells are distinct. This initial segmentation is then propagated over time to compute the segmentation of images acquired during hydrolysis. Thereby, WallTrack provides an automated high throughput 4D imaging pipeline devised to segment and track lignocellulose deconstruction at cell wall resolution leading to a detailed tissue-wide virtual representation of plant cell wall deconstruction. More precisely, let $\{I_{t_0}, \ldots, I_{t_n}\}$ denote the set of time-lapse three-dimensional (3D) confocal acquisitions (z-stacks) acquired during the enzymatic deconstruction of poplar samples, where I_{t_i} represents the i-th 3D confocal image acquired at time t_i for $0 \leqslant i \leqslant n$, and I_{t_n} denotes the final acquisition at time t_n, with $t_n = 24$ hrs in this study. I_{t_0} is referred to as the image before hydrolysis or pre-hydrolysis image in the Results and discussion section. The z-stacks contained empty slices and some noise in their top and bottom sections, with the poplar sample imaged in the middle section. Special care was taken to align the sample surface normal as closely as possible to the Z direction to avoid tilted subsequent acquisitions. To identify the imaged poplar sample within I_{t_0}, WallTrack first calculates the average signal intensity per voxel (volumetric pixel) for each slice. The imaged sample is then isolated by excluding the top and bottom slices whose average signal intensity per voxel is less than or equal to a manually defined threshold of 8. For segmenting the pre-hydrolysis image, WallTrack applies a 3D watershed algorithm (Willis et al., 2016), spatially constrained to the middle section of the pre-hydrolysis z-stack containing the imaged sample, following denoising with both a Gaussian filter and an alternative-sequential filter (ASF). The watershed seeds are computed using the h-minima operator by identifying local minima regions (Willis et al., 2016). WallTrack computes the cell wall segmentation of I_{t_0}, denoted by S_{t_0}, using thresholding, as follows:

$$S_{t_0}(i,j,k) = \begin{cases} 1 \text{ if} & I_{t_0}(i,j,k) < \tau \\ W_{t_0}(i,j,k) & \text{else} \end{cases},$$

where W_{t_0} is the watershed segmentation, and $i,j,k \in \mathbb{N}, i \leqslant M, j \leqslant N, k \leqslant K$, M, N, K are X-Y resolution, and number of image slices of I_{t_0} respectively. τ is a global threshold value selected manually and 1 is the background label in the segmented image. To segment the z-stacks during enzymatic hydrolysis, (i.e. I_{t_i}, $t_0 < t_i \leqslant t_n$), WallTrack first computes the affine transformation that linearly registered I_{t_0} onto I_{t_i} using block matching algorithm (Ourselin et al., 2000). WallTrack uses the affine transformation to initialize the block matching algorithm to compute the non-linear transformation $T_{t_0 \leftarrow t_i}$ to register I_{t_0} onto I_{t_i}, Fig. 1.A. This non-linear transformation, $T_{t_0 \leftarrow t_i}$, is then applied to the initial watershed segmentation to get $W_{t_i} = W_{t_0} \circ T_{t_0 \leftarrow t_i}$, Fig. 1.B. Thresholding is subsequently applied to determine the segmentation of the cell wall of I_{t_i} denoted by S_{t_i}:

$$S_{t_i}(i,j,k) = \begin{cases} 1 \text{ if} & I_{t_i}(i,j,k) < \tau \\ W_{t_i}(i,j,k) & \text{else} \end{cases},$$

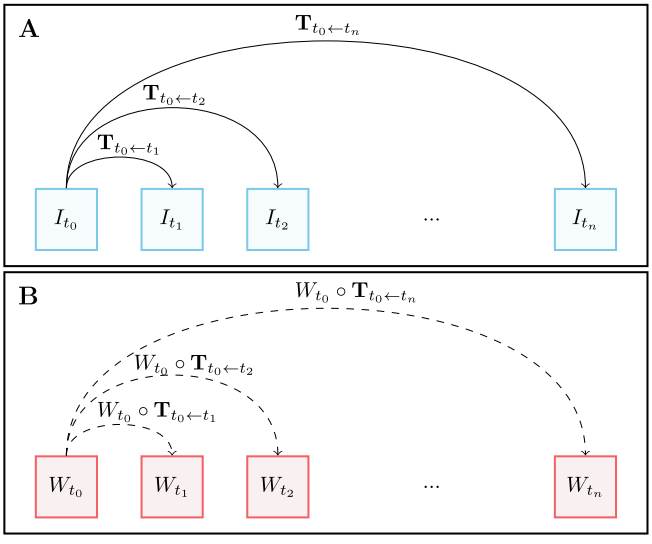

Fig. 1. Propagation strategy used in the segmentation and tracking pipeline to segment images during deconstruction. (A) The nonlinear transformations which register the image acquired prior to hydrolysis onto the images acquired during deconstruction are computed. (B) The propagation strategy used to compute the segmentation of the images acquired during hydrolysis involves the application of the computed transformation to the segmentation of the pre-hydolysis image.

where $i, j, k \in \mathbb{N}, i \leqslant M, j \leqslant N, k \leqslant K, M, N, K$ are X-Y resolution, and number of image slices of I_{t_i} respectively (see supplementary material).

The non-linear transformation $T_{t_0 \leftarrow t_i}$ allowing to register and resample I_{t_0} in the frame of I_{t_i} allows also to compute the 4D voxel resolution map of cell wall deconstruction where $I_{t_0} \circ T_{t_0 \leftarrow t_i}$ and I_{t_i}, for $t_0 < t_i \leqslant t_n$, are combined. This ensures that I_{t_0} is accurately aligned with I_{t_i}, thereby facilitating a direct comparison between the two images generating a voxel resolution deconstruction map, Fig. 2.

WallTrack presents significant advantages in achieving precise segmentation and minimizing the segmentation errors. Segmentation of the images during hydrolysis involves a single computation of a non-linear transformation to register the floating image (pre-hydrolysis image) and the reference image (the image during hydrolysis). Consequently, the segmentation is derived using a single resampling through the application of the transformation to the segmentation of the pre-hydrolysis image. This minimalist but efficient propagation strategy method avoids the complexities and potential inaccuracies associated with the composition of multiple transformations or the successive application of transformations, thus enhancing overall segmentation precision. However, the accuracy of WallTrack's segmentation during hydrolysis is dependent on the precision of the initial pre-hydrolysis image segmentation. Any errors in the segmentation of the pre-hydrolysis image could propagate through to subsequent images, emphasizing the importance of meticulous initial segmentation. Key to this initial accuracy are the parameters chosen for the denoising algorithms, the Gaussian filter and alternative-sequential filter (ASF), as well as the h-minima operator used to determine watershed seeds. Once these parameters are set for the initial pre-hydrolysis image, no additional adjustments are required for segmenting subsequent images in the same time-lapse sequence or any other images in different time-lapse datasets given the consistency of the microscope parameters across all time-lapse imaging.

To compute cell wall volume, voxel counting method was used where the number of voxels having the same label were computed and was multiplied by the voxel volume which was approximately 0.155 μm^3 due to the imaging resolution. The cells at the margins of the images together with small cell segments (whose volumes are typically smaller than 400 μm^3) which comprises the precision of quantification because of the movement of the sample during acquisition are discarded from the analysis. To compute cell wall surface area triangular meshes of cell wall surfaces were generated using the marching cubes algorithm from the Visualization Toolkit (VTK). To compute cell surface area triangular meshes were generated from watershed segmentations. The accessible surface area, ASA, was computed as $ASA = (A_w + A_l - A_c)/2$, where A_w, A_l, and A_c are cell wall surface area, lumen surface area, and cell surface area respectively. To compute average cell wall volumetric deconstruction rates, the average values of median values of cell wall volumetric deconstruction rates of each time-lapse were computed. WallTrack is implemented in Python 3 language using Numpy and Scipy packages.

3. Results and discussion

3.1. Automated segmentation and tracking of cell wall deconstruction

To assess the effectiveness of the dilute acid pretreatment method on the selected model biomass, poplar wood, the chemical compositions of both untreated and pretreated samples were analyzed. The chemical composition of the plant cell wall is important for the yield and rate of enzymatic hydrolysis. The analysis indicated a reduction in the fraction of hemicelluloses by approximately 3.2-fold due to the pretreatment (see supplementary material), in line with previous results (Zoghlami et al., 2019). Using plant cell wall natural autofluorescence (Donaldson and Radotic, 2013), time-lapse confocal images of poplar wood samples pretreated with dilute acid during enzymatic hydrolysis were collected following the protocol developed in (Zoghlami et al., 2020). Confocal images were acquired every thirty minutes for the first 4 h, followed by

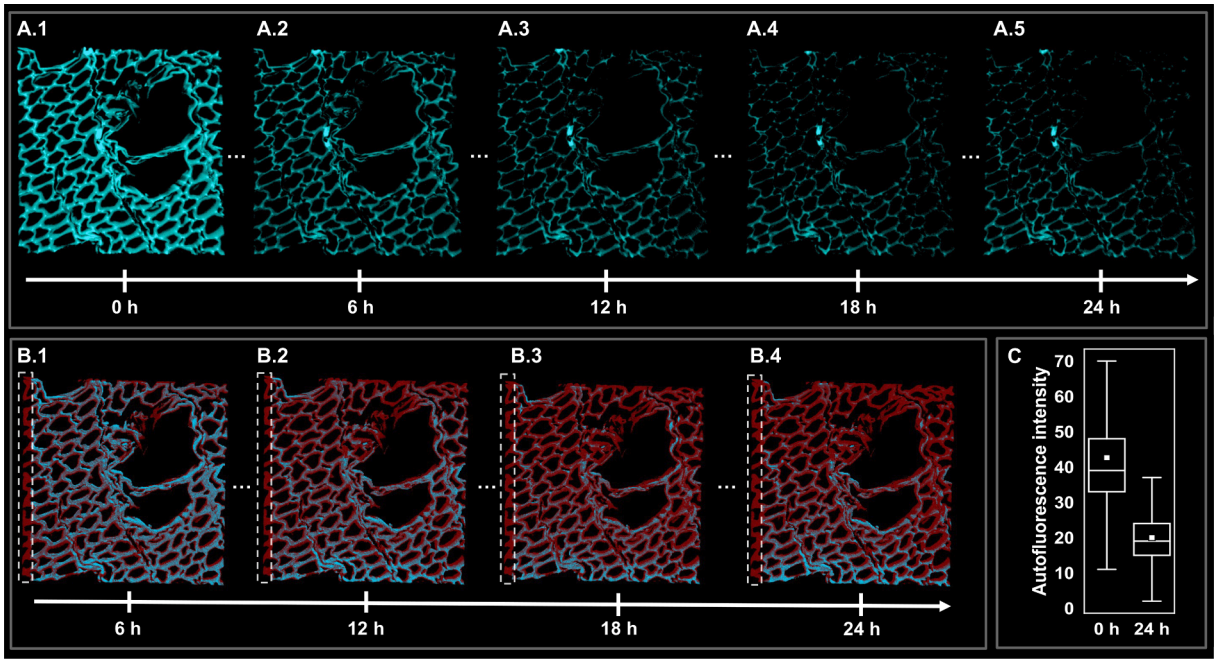

Fig. 2. 4D imaging of cell wall deconstruction during enzymatic hydrolysis using lignin autofluorescence. (A) Confocal time-lapse images of poplar wood sample were acquired every 30 min for the first 4 h followed by acquisitions every hour during enzymatic hydrolysis for the next 20 h (every 6 h is shown) with enzymatic activity of 20 FPU/ g glucan. (B) 4D voxel (voxel is a 3D pixel) resolution map of cell wall deconstruction (color code: red: deconstructed voxels, cyan: remaining voxels). The area delineated by the dotted rectangle represents the region that remained untracked due to sample displacement occurring throughout the imaging process. (C) Distributions of cell wall autofluorescence intensity before and after 24 h of enzymatic hydrolysis which show a significant reduction in autofluorescence intensity values (Anova, p-value < 0.005). The central lines of the box plot are the median values, and the white squares represent the average values. Image acquisition times are indicated below each image, followed by 'h' for hours.

hourly acquisitions for the next 20 h (Fig. 2.A). After acquiring these time-lapse confocal images, an original automated high-throughput 4D image segmentation and tracking pipeline, named WallTrack, was developed to quantitatively characterize cell wall deconstruction. WallTrack simultaneously accomplishes two tasks: i) It computes a 4D voxel (voxel indicates a 3D pixel) resolution map of cell wall deconstruction, despite the movement of the sample during imaging (Fig. 2.B), and allows for precise quantification of autofluorescence intensity before and after hydrolysis (Fig. 2.C). ii) It segments individual cell walls and tracks their evolution during enzymatic hydrolysis. WallTrack is devised to address the challenge of cell wall autofluorescence intensity loss during enzymatic hydrolysis, which renders classical segmentation methods unsuitable. Due to the deconstruction of the cell wall, holes and cracks appear in the early hours of enzymatic hydrolysis, potentially leading to the complete disintegration of cell wall segments between neighboring cells. This results in increased segmentation errors such as the fusion of neighboring cells (under-segmentation) or the division of an individual cell wall into multiple smaller, unnecessary segments (over-segmentation) when using classical segmentation methods (Fernandez et al., 2010; Willis et al., 2016). Furthermore, enzymatic deconstruction causes separation between the compound middle lamella and the secondary cell wall (Zoghlami et al., 2019), a process driven by the solubilization and breakdown of cell wall components that act as adhesives between layers (Ling et al., 2016). This separation can also lead to over-segmentation errors, where a cell is erroneously divided into two parts. Applying classical methods to datasets with low deconstruction (in early acquisitions with low enzymatic activity) where only cell wall thickness is reduced, requires manual adjustment of the denoising and segmentation algorithms' parameters to segment each acquisition in the time-lapse datasets. This manual tuning is time-consuming and impractical for large datasets, as each individual acquisition must be checked for segmentation errors. Alterations in parameter values can impact quantifications and therefore can introduce bias, lead to compromised accuracy and reliability, and thereby reduce objectivity. WallTrack addresses these significant limitations by propagating the 3D segmentation of the image before hydrolysis to compute the segmentation of images acquired during hydrolysis. This strategy of propagating spatial information over time, first used on living organisms (Amat et al., 2014), allows the identification of individual deconstructed cell walls using their earlier state, where the cell walls are intact and the cell boundaries between neighboring cells are clearly marked (i.e. before enzymatic deconstruction). WallTrack first computes the cell wall resolution segmentation of the acquired confocal image before hydrolysis using watershed algorithm and threshdoling (Fig. 3.A). Subsequently, WallTrack registers the acquired confocal image before hydrolysis with the subsequent confocal images to compute the transformations (Fig. 1.A). The transformations are then applied to the pre-hydrolysis cell segmentation obtained using watershed algorithm to compute cell segmentations of hydrolysis phase confocal acquisitions (Fig. 1.B, and (see supplementary material)). Finally, the cell wall segmentations are computed using thresholding (Fig. 3.B). By employing this approach, WallTrack automatically generates 3D segmentation of individual cell walls at each time point with unique cell wall identifiers, which remain consistent over time, thereby enabling tracking and analysis of the cell walls during deconstruction.

3.2. *Cell scale impact of enzymatic deconstruction predominantly manifests as a reduction in cell wall volume rather than a reduction in cell wall accessible surface area*

To investigate the spatio-temporal cell and tissue scale structural changes during enzymatic deconstruction, an adjacency graph representing the tissular organization and structure was first computed from the segmented 4D images generated by WallTrack. In the adjacency graph, vertices represent the cells and edges represent cell walls or shared boundaries between neighboring cells (Fig. 4.A). The degrees of the vertices in the adjacency graph were then computed, indicating the number of neighboring cells for each cell, or the number of distinct cell walls that are shared with adjacent cells (Koutrouli et al., 2020; Bilgin et al., 2007). For an individual cell, the number of cell neighbors is equivalent to the number of cell junctions which exhibit a unique composition compared to other parts of the cell wall, typically having a

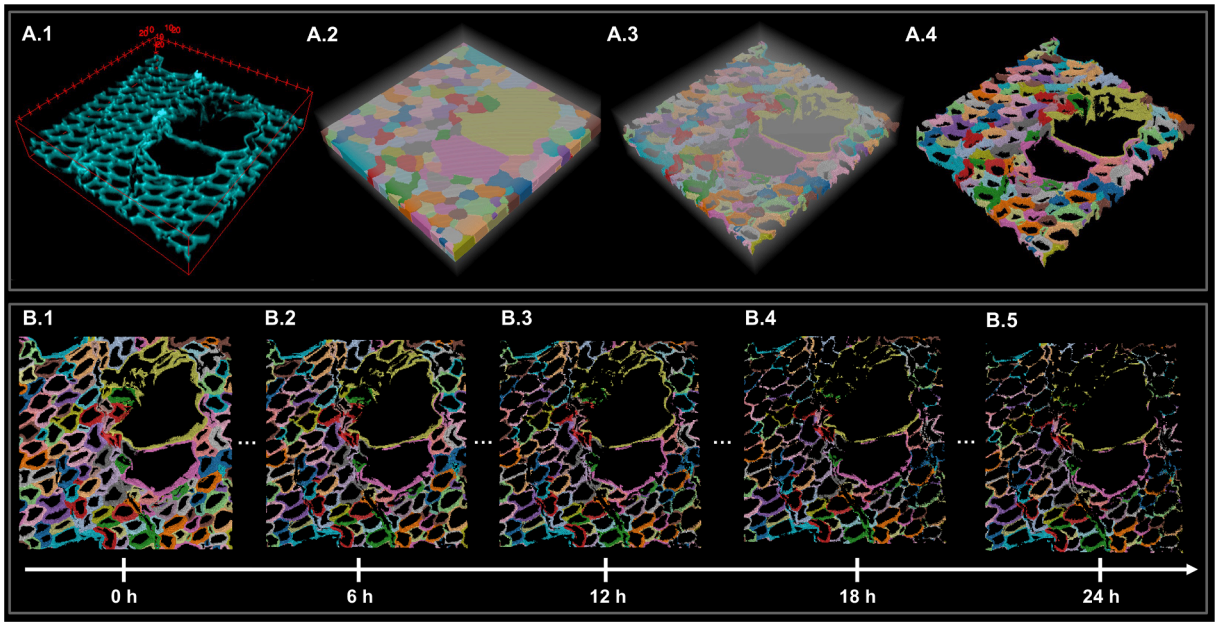

Fig. 3. 4D segmentation and tracking of cell walls during enzymatic hydrolysis. (A) Segmentation of the image before hydrolysis. (A.1) Confocal acquisition before enzymatic hydrolysis (A.2) Cell resolution segmentation of the image before enzymatic hydrolysis obtained using watershed algorithm with auto seeding. The background is marked by a semi-transparent white color. (A.3) Cell wall segmentation obtained using thresholding. (A.4) Background removal. The cells and cell walls are colored randomly to facilitate the visual distinction of neighboring cells. (B) Cell wall segmentation and tracking of the confocal time-lapse images shown in (Fig. 2.A). The cell wall segmentation is obtained after thresholding of propagated cell segmentations. (every 6 h is shown: C.1 – 5 correspond to the images shown in (Fig. 2.A.1 – 5)). Cell walls are colored accord.ing to lineages.

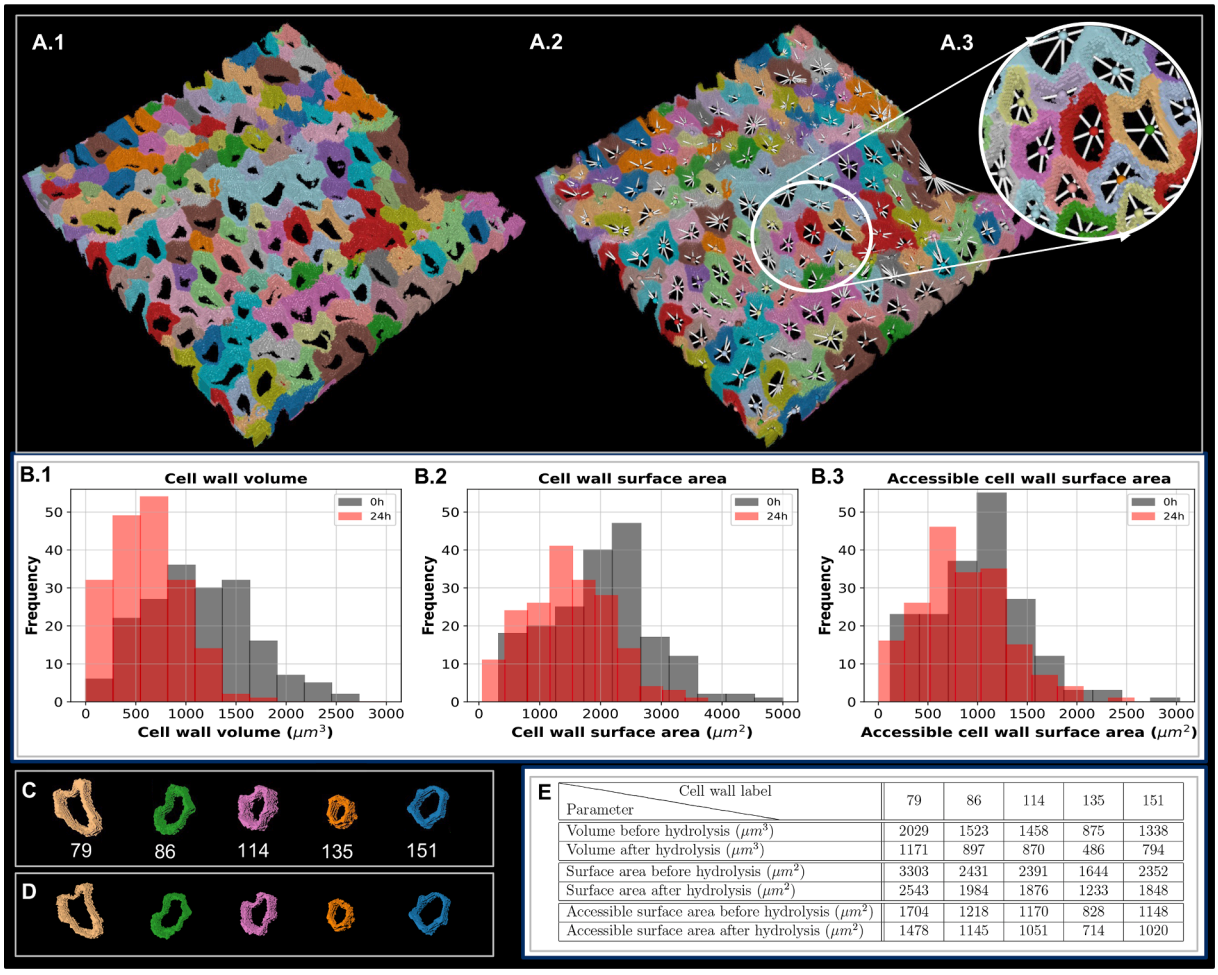

E

Parameter \ Cell wall label	79	86	114	135	151
Volume before hydrolysis (μm^3)	2029	1523	1458	875	1338
Volume after hydrolysis (μm^3)	1171	897	870	486	794
Surface area before hydrolysis (μm^2)	3303	2431	2391	1644	2352
Surface area after hydrolysis (μm^2)	2543	1984	1876	1233	1848
Accessible surface area before hydrolysis (μm^2)	1704	1218	1170	828	1148
Accessible surface area after hydrolysis (μm^2)	1478	1145	1051	714	1020

Fig. 4. Quantification of cell and tissue scale parameters during enzymatic hydrolysis. (A) Extraction of adjacency graph from segmented images. Cell adjacency graph represents the tissue's structure and its intercellular connections by a graph computed from the segmented image (A.1). Cells are represented as nodes (vertices), and shared cell walls are represented by edges between neighboring cells (A.2) in the adjacency graph. (B) Cell and tissue scale parameter quantification before and after hydrolysis (B.1) Cell wall volume distribution before and after 24 h of hydrolysis. We can observe a statistically significant shift to the left of the distribution of cell wall volumes after hydrolysis (Anova test, p-value < 0.005, N $= 184$) (B.2) Distributions of cell wall surface areas of individual cells before and after 24 h of hydrolysis (N $= 184$). (B.3) Distributions of accessible cell wall surface areas before and after 24 h of hydrolysis (N $= 184$). (C) Randomly selected cell walls before hydrolysis with their unique identifiers (labels) shown in the row directly below. (D) The selected cell walls during hydrolysis which exhibit changes due to enzymatic hydrolysis (E) Cell wall volume, surface area, and accessible surface area before and after hydrolysis for the selected cells shown in C and D.

higher lignin content (Zhao et al., 2012a; Agarwal, 2006). After determining the adjacency graph, attention was focused on the cell wall volume and cell wall surface area as two key indicators of size at cell scale. This focus was prompted by visual observations of individual cells during hydrolysis, which highlighted changes in cell volumes and cell wall surface areas (Fig. 3.B.1 – B.5 and Fig. 4.C & D). Thus, the individual cell wall volumes were computed using the segmented time-lapse images. A significant reduction of the cell wall volume after 24 h of hydrolysis was observed for all time-lapse datasets collected in the presence of enzymes (Anova test, p-value < 0.005) (Fig. 4.B.1 & E). The total surface area of the cell walls were then computed (Fig. 4.B.2 & E). The surface area directly influences the enzyme-substrate interactions since enzymes require adequate access to their target substrates within the complex lignin-embedded polysaccharide matrices (Thompson et al., 1992).

A general reduction in the total surface area was observed, however, a conclusive statistically significant difference between the surface area before and after 24 h of enzymatic deconstruction was not found. The accessible surface area (ASA) was then computed by taking into account the wall surface regions which are directly in contact with enzymes and discarding the cell walls shared by neighboring cells. The cell wall accessible surface area can be seen as a cell scale counterpart to the accessible surface area of the cell wall polysaccharide matrix (the higher accessible cell wall surface, the higher accessibility to polysaccharides) and is one of the most important parameters affecting the plant cell wall enzymatic deconstruction yield and rate (Meng and Ragauskas, 2014; Meng et al., 2015). Similar to the total surface area, a reduction was observed in the accessible surface area which was not statistically conclusive (Fig. 4.B.3 & E). The cell wall volume representing the 3D space occupied by the lignocellulosic constituents of the cell, and its evolution during enzymatic deconstruction were consequently chosen as the size metric providing a quantifiable cell scale indicator to characterize the enzymatic deconstruction of the cell wall.

3.3. Three dimensional cell wall compactness measures prior to hydrolysis are correlated with volumetric cell wall deconstruction rate whose strength is modulated by the enzymatic activity

Building upon the quantification of cell wall volume and cell wall surface area, further investigation was conducted on the cell and tissue scales parameters to study whether they can be informative about the enzymatic deconstruction at cell and tissue scales. More precisely, the study investigated whether the pre-hydrolysis cell and tissue scale parameters (i.e. parameters measured prior to enzymatic deconstruction)

can potentially serve as predictive markers for volumetric cell wall deconstruction rate. The numbers of individual cells analyzed before hydrolysis were 185, 177, 205, and 202 for datasets collected with enzymatic activity of 0 FPU/ g glucan, 5 FPU/ g glucan, 10 FPU/ g glucan, and 20 FPU/ g glucan, respectively. The total number of cells in the time-lapse datasets analyzed were 5180, 4956, 5740, and 5656 for datasets collected with enzymatic activity of 0 FPU/ g glucan, 5 FPU/ g glucan, 10 FPU/ g glucan, and 20 FPU/ g glucan, respectively. The volumetric cell wall deconstruction rate after 24 h of enzymatic hydrolysis, denoted hereafter by D^{24h}, is defined as $D^{24h} = (V_w^{0h} - V_w^{24h})/(V_w^{0h} \times 24)$, where V_w^{0h} and V_w^{24h} are cell wall volumes before and after 24 h of enzymatic deconstruction respectively. The Pearson correlation was first computed between cell wall volume before hydrolysis, V_w^{0h}, and D^{24h}, for the datasets collected in the absence (0 Filter Paper Units (FPU)/ g glucan) and in the presence of enzymes with three different enzyme loadings of 5, 10, and 20 FPU/g glucan (Fig. 5.A.1 – 4). This range of enzymatic activities was selected to represent varying levels and to examine their effects on cell wall deconstruction.A very weak positive correlation was observed for datasets collected with the highest enzymatic activity value (20 FPU/ g glucan), and a very weak negative correlation for the datasets collected in the absence of enzymes, with no significant correlations for datasets collected with other enzymatic activities (5 and 10 FPU/ g glucan). The Pearson correlation was then computed between the number of cell neighbors and D^{24h}. A weak negative correlation was observed exclusively for the datasets collected with enzymatic activity value of 20 FPU/ g glucan. To investigate the relationship between surface area and volumetric cell wall deconstruction rate, the Pearson correlations were then computed between D^{24h} and the total cell wall surface area and cell wall accessible surface area before deconstruction. Weak positive correlations were identified for the highest enzymatic activity values (10 and 20 FPU/ g glucan) for both pre-hydrolysis total cell wall surface area and accessible cell wall surface area, with higher correlation coefficients for pre-hydrolysis accessible surface area compared to the coefficients computed for pre-hydrolysis total surface area. To sum up, the correlations between initial cell wall volume, number of adjacent cells, cell wall surface area, and accessible cell wall surface area were not conclusively correlated with volumetric cell wall deconstruction rate. Consequently, the focus was redirected to investigate the relationship between the compactness of the cell wall before hydrolysis, quantified as a ratio of cell wall volume to cell wall surface area, and its volumetric deconstruction. The cell wall compactness at level of polymers' matrix is essentially connected to the density and arrangement of polymers (mainly cellulose, hemicelluloses, and lignin) within the cell wall structure. Consequently, compactness is linked to the restricted enzymatic accessibility to polysaccharide fibers due to the tight packing of the wall components (Meng et al., 2017). Therefore, the cell wall Compactness Index (*CI*), a dimensionless parameter which is the ratio of volume over the total surface area raised to the power of three-halves, was first computed (Fig. 5.C). The definition of *CI* implies that if two

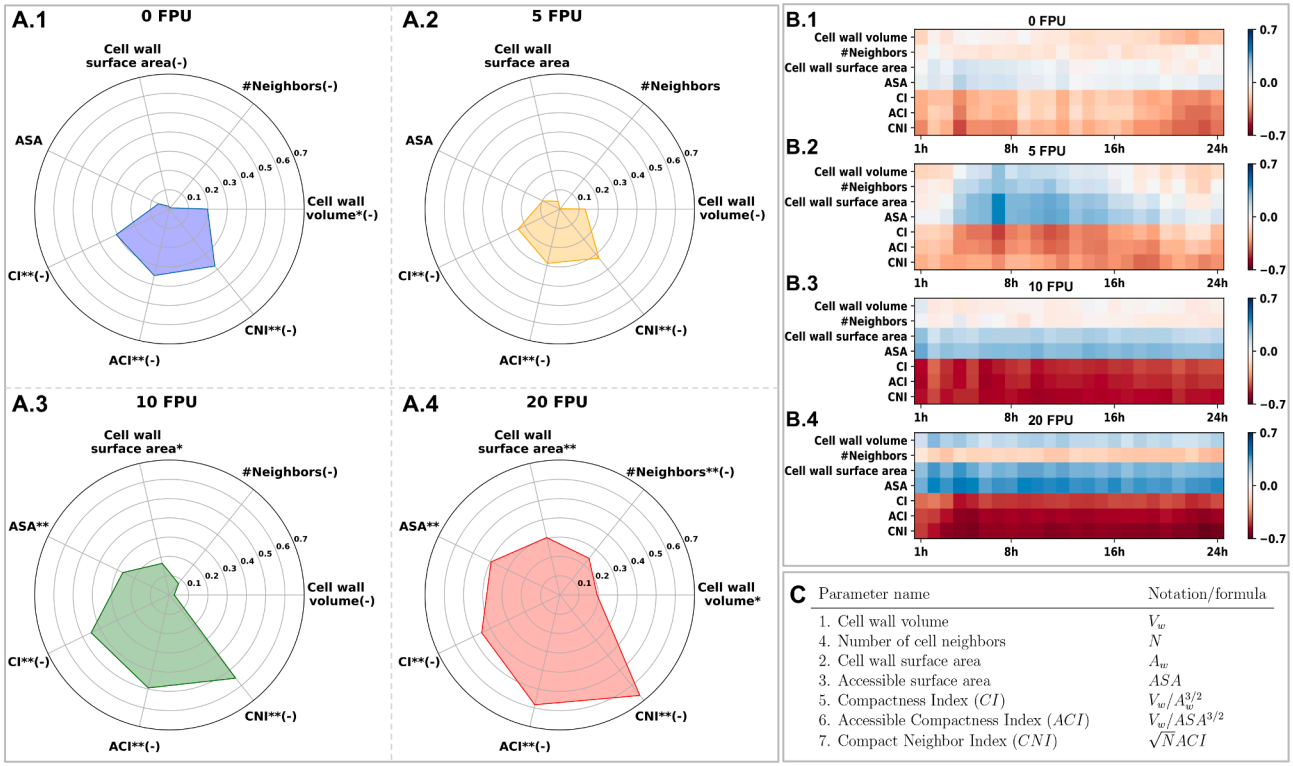

Fig. 5. Correlation coefficient values between cell and tissue scale parameters prior to enzymatic deconstruction and volumetric cell wall deconstruction rate. (A.1) Pearson correlation coefficient values between volumetric cell wall deconstruction rate after 24 h of enzymatic hydrolysis and initial cell and tissue scale parameters in the absence of enzymes. (A.2 – 4) Pearson correlation coefficient values between volumetric cell wall deconstruction rate after 24 h of enzymatic hydrolysis and pre-hydrolysis cell and tissue scale parameters in the presence of enzymes with enzymatic activity of 5, 10, and 20 FPU/ g glucan respectively. (B.1) Correlation matrix showing correlation coefficients between volumetric cell wall deconstruction rate during enzymatic hydrolysis for 24 h and initial cell and tissue scale parameters in the absence of enzymes (0 FPU/ g glucan). (B.2 – 4) Correlation matrix showing correlation coefficients between volumetric cell wall deconstruction rate during enzymatic hydrolysis for 24 h and pre-hydrolysis cell and tissue scale parameters in the presence of enzymes for enzymatic activities of 5, 10, and 20 FPU/ g glucan respectively. (C) Table of notations and formulas for cell and tissue scales parameters. Accessible Surface Area denotes the accessible cell wall surface area. (-) denotes negative correlations and statistical significance of correlation coefficients are marked with * and ** for p-value < 0.05 and p-value < 0.005 respectively. Numbers of individual cells before hydrolysis are 185, 177, 205, and 202 for datasets collected with enzymatic activity of 0 FPU/ g glucan, 5 FPU/ g glucan, 10 FPU/ g glucan, and 20 FPU/ g glucan respectively. Total number of cells in the time-lapse datasets analyzed in B.1 – B.4 are 5180, 4956, 5740, and 5656 for datasets collected with enzymatic activity of 0 FPU/ g glucan, 5 FPU/ g glucan, 10 FPU/ g glucan, and 20 FPU/ g glucan respectively.

cell walls have the same volume, the one with a smaller surface area is more compact. Significant negative correlations were identified between *CI* and D^{24h} in datasets collected in the presence and absence of enzymes (Fig. 5.A.1 – 4). The Accessible Compactness Index (*ACI*) was then computed where the accessible cell wall surface area is used rather than the total surface area to determine the cell wall compactness (Fig. 5.C). Significant negative correlations were found between *ACI* and D^{24h} in the presence and absence of enzymes with higher correlation coefficients compared to those obtained between *CI* and D^{24h}. Building on this result, the approach was further refined by incorporating the number of cell neighbors into the compactness calculation, resulting in a parameter that is called Compactness Neighbor Index and denoted as *CNI*. This integration aimed to account for the potential influence of surrounding cells on the deconstruction process, hypothesizing that the local cellular environment might play a role in determining the susceptibility of the cell wall to enzymatic deconstruction. The rationale behind this was that the number of neighboring cells could be indicative of the compactness at the tissue scale, providing insights into how closely packed cells within a tissue can affect enzymatic access and efficiency. *CNI* was computed by multiplying *ACI* by the square root of the number of neighboring cells. Remarkably, the inclusion of the number of cell neighbors into the compactness metric yielded even more pronounced results. A higher correlation was observed between *CNI* and volumetric cell wall deconstruction rate compared to *ACI* alone (Fig. 5. A.1 – 4). This enhanced correlation indicates that *CNI* appears to be a more reliable predictor of volumetric cell wall deconstruction rate and underlines the importance of the intercellular context in which enzymatic deconstruction occurs. Furthermore, the comparison of correlation coefficients of different parameters computed for the data collected in the absence of enzymes and in the presence of enzymes with different activities revealed that the strength of correlations is modulated by the level of enzymatic activity such that the strength of the correlation coefficients increased with higher enzymatic activity. The difference between the correlation coefficients between the control datasets and the datasets collected with enzymatic activity of 5 FPU/ g glucan was not significant. The Pearsoncorrelation was then computed between cell wall volume, cell wall surface area, number of neighbors, ASA, CI, ACI, CNI prior to deconstruction and volumetric cell wall deconstruction rate during hydrolysis, i.e. $D^t = (V_w^{0h} - V_w^t)/(V_w^{0h} \times t)$, $0h < t \leqslant 24h$ where V_w^{0h} and V_w^t are cell wall volumes before and after t h of enzymatic deconstruction respectively (Fig. 5.B.1 – 4). The results revealed the same statistical trends with no conclusive correlations between D^t and the pre-hydrolysis cell wall volume, number of cell neighbors, cell wall surface area, and accessible cell wall surface area. Significant negative correlations between pre-hydrolysis compactness parameters (i.e. CI, ACI, and *CNI*) and volumetric cell wall deconstruction rate were consistently observed across different time intervals within the 1 to 24 h range of enzymatic deconstruction. The higher enzyme activities consistently led to stronger correlations for $D^t, 1 < t \leqslant 24$ hrs. This consistency across various time points underscores the robustness of the cell scale compactness metrics, CI, ACI, and *CNI*, in capturing key structural determinants of cell wall deconstruction over the course of enzymatic activity.

3.4. Average volumetric cell wall deconstruction rate is strongly correlated with cellulose conversion rate

To validate the reproducibility of the hydrolysis conditions in the mini-reactors, hydrolysis yields of poplar samples were determined in both the mini reactors and the sealed frames (identical as that used for 4D imaging). Indeed, the sealed frames cannot be used routinely for cellulose conversion analysis since they need to be broken to recover the reaction medium to quantify monosaccharides released. For this validation test, an enzymatic loading of 10 FPU/g of glucan and a final time point of 24 h were chosen as standard conditions. Results showed that hydrolysis yields were highly similar: 12.0% ± 0.2% and 11.2% ± 0.3 for the mini-reactor and the sealed frame, respectively. This shows that the mini reactor system can be a reliable proxy for replicating the enzymatic hydrolysis environment of sealed frames. In order to elucidate the connection and interplay between parameters at the polymer and cell scales, cellulose conversion in poplar sections could confidently be followed within mini-reactors over a 24-h period and the cellulose conversion with three enzyme loadings of 5, 10, and 20 FPU/ g glucan was determined. The measurements indicated a marked increase in cellulose conversion during the initial 4 h, followed by a more gradual rise in the subsequent 20 h, suggesting a slowdown in the enzymatic process (see supplementary material). It was also observed that higher enzyme loading levels corresponded to increased rates of cellulose conversion. In contrast, experiments conducted in the absence of enzymes yielded significantly lower cellulose conversion rates. These results were in line with the expected outcomes and previous research (Ju et al., 2013; Hodge et al., 2008).

Consequently, a quantitative relationship between the cellulose conversion and the volumetric cell wall deconstruction was sought. For this purpose, a regression analysis was performed which revealed robust linear relationships with strong Pearson correlation coefficients ranging from 0.979 to 0.998 and highly significant p-values (< 0.0001) between the cellulose conversion rate and the average volumetric cell wall deconstruction rate during hydrolysis for all enzymatic activities. These results, illustrated in Fig. 6, underscore a quantifiable linear relationship that bridges nano-scale cellulose conversion with micro-scale cell and tissue scales cell wall deconstruction. Moreover, this result demonstrates that the volumetric deconstruction of cell walls is a relevant indicator of the deconstruction of the plant cell wall into glucose. This aspect is particularly crucial in the context of the saccharification process, where the efficiency of converting plant biomass into simple sugars is of paramount importance.

3.5. Bridging scales: Cross-scale insights, key implications, and application perspectives

One of the key achievements of this study is the development of the WallTrack pipeline, which facilitates the automated, high-throughput, quantitative analysis of cell and tissue-scale dynamics in cell wall deconstruction. WallTrack addresses the challenges associated with the reduction in the cell wall autofluorescence intensity due to the change in lignin environment and the physical instability of the sample occurring during enzymatic hydrolysis. WallTrack also enhances the precision and reliability of the segmentation through automation, reducing human error and bias. WallTrack generates a detailed tissue-wide virtual representation of enzymatic deconstruction, representing a significant step towards creating a digital twin of lignocellulose deconstruction. This digital twin will integrate the 4D virtual tissue provided by WallTrack, serving as an accurate digital representation and mapping of its real-world counterpart (Tao et al., 2022). By incorporating spatio-temporal computational models of enzymatic deconstruction, this digital twin can simulate in vitro experiments, and therefore can serve as a powerful decision support tool for optimizing the enzymatic deconstruction of plant cell walls.

The findings shed light on the relationship between pre-hydrolysis 3D cell wall architecture and its susceptibility to enzymatic deconstruction. A significant negative correlation was identified between cell wall compactness and volumetric deconstruction rate, with the strength of the correlation modulated by the level of enzymatic activity. This indicates that cell wall compactness, as a parameter combining cell wall volume and cell surface area, is a more reliable indicator of volumetric cell wall deconstruction rate compared to the cell wall volume and cell wall surface area taken alone. A more compact cell wall can be more resistant to pretreatment and enzymatic deconstruction because the tight packing of cellulose, hemicelluloses, and lignin makes it more difficult for enzymes to access and break down these polymers

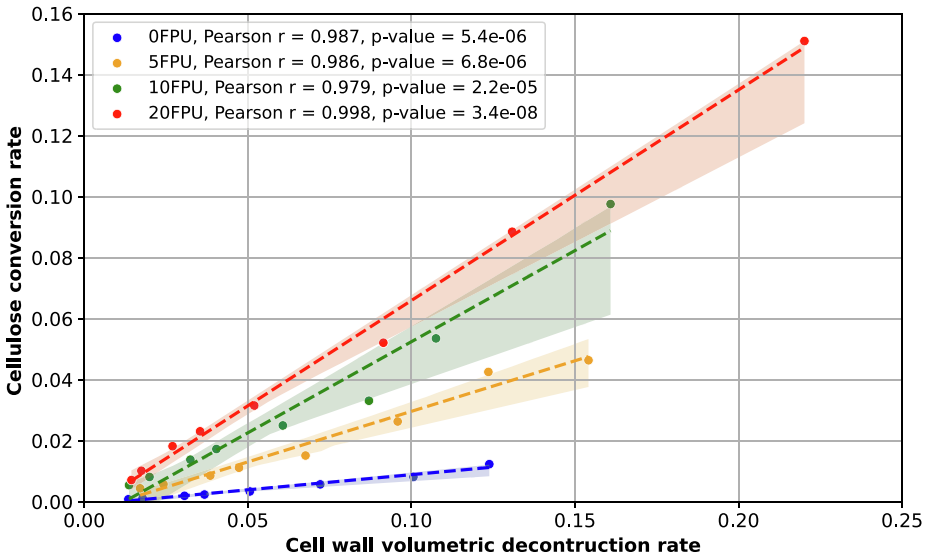

Fig. 6. Average volumetric cell wall deconstruction rates versus cellulose conversion rates. The dashed lines represent the linear regression and the shaded areas represent the confidence intervals. The data points are shown with different colors (0 FPU/g glucan - blue, 5 FPU/g glucan - orange, 10 FPU/g glucan - green, 20 FPU/g glucan - red). The legend provides the Pearson correlation coefficients (r) and p-values for each enzymatic activity level, demonstrating a strong positive correlation in all cases.

(Zoghlami et al., 2019). The negative correlation of the number of cell neighbors with volumetric cell wall deconstruction rate, particularly at high enzymatic activities, aligns with the fact that a higher number of cell neighbors implies a higher number of lignin-concentrated recalcitrant cell junctions (Zhao et al., 2012a; Zhao et al., 2012b; Agarwal, 2006) supporting the inverse relationship between the number of neighbors and volumetric cell wall deconstruction rate. Consequently, the integration of the number of neighbors and cell wall compactness, *CNI* parameter, led to stronger correlations regardless of level of enzymatic activity. This provides a single dimensionless parameter integrating both cell scale (compactness) and tissue scale parameter (number of neighbors) as an indicator of volumetric cell wall deconstruction rate. The use of the square root transformation suggests that while the presence of neighboring cells impacts deconstruction, this impact does not increase linearly with their number and the impact of each additional neighbor becomes progressively smaller, underscoring a non-linear relationship. Dimensionless parameters are highly relevant because they allow comparison of results across different time-lapse datasets which can have different sizes and dimensions and facilitate the scaling of computational results to real-world, full-scale applications, ensuring that derived insights are applicable across various sizes and conditions.

Moreover, a more intricate relationship between cell wall compactness measures and volumetric cell wall deconstruction rate was identified, where the strength of the correlation is modulated by the level of enzymatic activity and a higher level of enzymatic activity corresponds to an increased correlation coefficient. This shows that the level of enzymatic activity clarifies and enhances the relationship between key parameters. Thus, in comprehensive predictive analysis of tissue scale cell wall deconstruction, the consideration of level of enzymatic activity is critical.

Importantly, the results revealed a strong and compelling correlation between average volumetric cell wall deconstruction rate and cellulose conversion rate. This finding indicates a measurable, linear connection that links the molecular-level transformation of cellulose to changes at the cell scale in cell wall volume. Moreover, this outcome underscores that the volumetric deconstruction of cell walls is a relevant indicator of the deconstruction of the plant cell wall into glucose. This aspect is particularly crucial in the context of the saccharification process, where the efficiency of converting plant biomass into simple sugars is of paramount importance. This quantitative relationship illustrates the potential, the relevance and the importance of studying enzymatic deconstruction at cell and tissue scales and advantageously completes previous studies aiming at deciphering the mode of action of enzymes, particularly cellulases at the nanoscale, with the limitation that only model cellulose was used (Bubner et al., 2012; Igarashi et al., 2011).

The identified correlations are supported by recent work on nanoscale cellulose digestion, which highlighted the role of amorphous cellulose regions as critical breakpoints for initiating and completing cellulose nanofibers saccharification and found that nanofibrils with more amorphous regions lead to enhanced enzymatic saccharification and higher sugar yields (Zhang et al., 2023c; Zhang et al., 2023b; Ai et al., 2024). These insights align with the observed negative correlation between pre-hydrolysis compactness measures and volumetric cell wall deconstruction: more compact cell walls likely have fewer accessible amorphous regions, making them more resistant to enzymatic hydrolysis, thus limiting enzyme action. Additionally, these results on the role of the amorphous regions in driving efficient hydrolysis support the positive correlation between cell wall volumetric deconstruction and cellulose conversion: the greater volumetric cell wall deconstruction exposes more amorphous regions, facilitating more efficient enzymatic conversion which directly supports the observed positive correlation. Furthermore, the findings of this study align with the impact of pretreatment on poplar wood. The significant reduction in hemicellulose and disruption of the compact cell wall structure after pretreatment expose more amorphous cellulose regions, increasing their accessibility to enzymes. This enhanced accessibility further supports the observed strong positive correlation. These insights into the role of amorphous cellulose regions, combined with findings of this study, provide a deeper mechanistic understanding of how nano-scale cellulose properties influence deconstruction dynamics at both the cell and tissue scales.

Even though this study is specific to pretreated poplar wood sections, it represents first evidence of a quantitative link between nano- and micro-scale markers on real biomass samples. Extending and transposing these observations to biorefinery cm-scale biomass fragments seems plausible given that these objects can be assimilated as a large stack of microsections, where only diffusion of enzymes (which influences only their kinetics) is modified. But the composition and organization of cell wall polymers are identical in both kinds of samples so the deconstruction mechanisms are highly similar. The conclusions thus

remain fully relevant and transferable at the industrial scale, given that diffusion of enzymes can be modeled. Also, it is important to note that this study is the first example of time-lapse hydrolysis performed on deconstructed 3D samples rather than on two-dimensional samples, which is a dramatic methodological advancement in focusing on real-life samples. Further research is essential to evaluate the generality of cell-scale markers across different biomass types and pretreatment methods combinations to assess the consistency of the markers. Extending this research in this direction is critical for developing a more comprehensive understanding of lignocellulose deconstruction across various feedstocks and pretreatment conditions. Since the enzymatic hydrolysis is a critical step in the conversion of plant cell wall into bio-based products, the finding of this significant robust relationship paves the way to better understand the saccharification. Indeed, synergy and interplay between hydrolases and oxidases such as LPMOs acting on lignocellulose is still under debate considering optimal partnering (Sørlie et al., 2023) while spatial localization of LPMO action at the cellular scale has been rarely investigated (Chabbert et al., 2017). Overall, the established strategy in this study should contribute to open and develop new paths for addressing these fundamental enzymatic questions.

4. Conclusions

Conversion of lignocellulosic biomass into bioproducts offers a promising solution for developing bioeconomy. In this study, an innovative computational pipeline is devised to better understand cell wall deconstruction at under-investigated cell and tissue scales. The pipeline was employed to analyze poplar wood sections hydrolysis, revealing a correlation between pre-hydrolysis cell wall compactness and volumetric cell wall deconstruction rate. Furthermore, a strong positive correlation was observed between the average volumetric deconstruction rate and the cellulose conversion rate, thus establishing a link between key parameters and bridging the gap between nano and micro scales.

Declaration of Competing Interest

The authors declare that they have no known competing financial interests or personal relationships that could have appeared to influence the work reported in this paper.

Data availability

The WallTrack code is accessible through the FARE laboratory GitLab repository at: https://gitlab.com/farelab/teamyr/publications/refahi_et_al_4d. Data will be made available on request.

Acknowledgments

The authors thank Anouck Habrant for her help in confocal imaging and Grégoire Malandain, Solmaz Hossein Khani, Khadidja Ould Amer, and Ali Faraj for their comments on the manuscript. This work was supported by Agence Nationale de la Recherche (ANR) through "BIO-MOD" (ANR-19-CE43-0010) grant to Y.R, and by Grand Est Region and FEDER through "TECMI-4D" PhD funding to A.Z.

Appendix A. Supplementary data

Supplementary data to this article can be found online at https://doi.org/10.1016/j.biortech.2024.131551.

References

Agarwal, U.P., 2006. Raman imaging to investigate ultrastructure and composition of plant cell walls: distribution of lignin and cellulose in black spruce wood (picea mariana). Planta 224, 1141–1153. https://doi.org/10.1007/s00425-006-0295-z.

Ai, Y., Wang, H., Liu, P., Yu, H., Sun, M., Zhang, R., Tang, J., Wang, Y., Feng, S., Peng, L., 2024. Insights into contrastive cellulose nanofibrils assembly and nanocrystals catalysis from dual regulations of plant cell walls. Sci. Bull. https://doi.org/10.1016/j.scib.2024.06.013.

Amat, F., Lemon, W., Mossing, D.P., McDole, K., Wan, Y., Branson, K., Myers, E.W., Keller, P.J., 2014. Fast, accurate reconstruction of cell lineages from large-scale fluorescence microscopy data. Nat. Methods. 11, 951–958. https://doi.org/10.1038/nmeth.3036.

Antar, M., Lyu, D., Nazari, M., Shah, A., Zhou, X., Smith, D.L., 2021. Biomass for a sustainable bioeconomy: an overview of world biomass production and utilization. Renew. Sustain. Energy. Rev. 139, 110691. https://doi.org/10.1016/j.rser.2020.110691.

Ashokkumar, V., Venkatkarthick, R., Jayashree, S., Chuetor, S., Dharmaraj, S., Kumar, G., Chen, W.H., Ngamcharussrivichai, C., 2022. Recent advances in lignocellulosic biomass for biofuels and value-added bioproducts-a critical review. Bioresour. Technol. 344, 126195. https://doi.org/10.1016/j.biortech.2021.126195.

Bilgin, C., Demir, C., Nagi, C., Yener, B., 2007. Cell-graph mining for breast tissue modeling and classification. In: in: 2007 29th Annual international conference of the IEEE Engineering in Medicine and Biology Society. IEEE, pp. 5311–5314. https://doi.org/10.1109/iembs.2007.4353540.

Binder, J.B., Raines, R.T., 2010. Fermentable sugars by chemical hydrolysis of biomass. Proc. Natl. Acad. Sci. U.S.A. 107, 4516–4521. https://doi.org/10.1073/pnas.0912073107.

Bubner, P., Dohr, J., Plank, H., Mayrhofer, C., Nidetzky, B., 2012. Cellulases dig deep: in situ observation of the mesoscopic structural dynamics of enzymatic cellulose degradation. JBC 287, 2759–2765. https://doi.org/10.1074/jbc.M111.257717.

Chabbert, B., Habrant, A., Herbaut, M., Foulon, L., Aguié-Béghin, V., Garajova, S., Grisel, S., Bennati-Granier, C., Gimbert-Herpoël, I., Jamme, F., et al., 2017. Action of lytic polysaccharide monooxygenase on plant tissue is governed by cellular type. Sci. Rep. 7, 17792. https://doi.org/10.1038/s41598-017-17938-2.

Donaldson, L., Radotic, K., 2013. Fluorescence lifetime imaging of lignin autofluorescence in normal and compression wood. J. Microsc. 251, 178–187. https://doi.org/10.1111/jmi.12059.

Fernandez, R., Das, P., Mirabet, V., Moscardi, E., Traas, J., Verdeil, J.L., Malandain, G., Godin, C., 2010. Imaging plant growth in 4d: robust tissue reconstruction and lineaging at cell resolution. Nat. Methods. 7, 547–553. https://doi.org/10.1038/nmeth.1472.

Guignard, L., Fiúza, U.M., Leggio, B., Laussu, J., Faure, E., Michelin, G., Biasuz, K., Hufnagel, L., Malandain, G., Godin, C., et al., 2020. Contact area–dependent cell communication and the morphological invariance of ascidian embryogenesis. Science 369, eaar5663. https://doi.org/10.1126/science.aar5663.

Haldar, D., Purkait, M.K., 2021. A review on the environment-friendly emerging techniques for pretreatment of lignocellulosic biomass: Mechanistic insight and advancements. Chemosphere 264, 128523. https://doi.org/10.1016/j.chemosphere.2020.128523.

Hall, M., Bansal, P., Lee, J.H., Realff, M.J., Bommarius, A.S., 2010. Cellulose crystallinity–a key predictor of the enzymatic hydrolysis rate. FEBS. J. 277, 1571–1582. https://doi.org/10.1111/j.1742-4658.2010.07585.x.

Herbaut, M., Zoghlami, A., Habrant, A., Falourd, X., Foucat, L., Chabbert, B., Paës, G., 2018. Multimodal analysis of pretreated biomass species highlights generic markers of lignocellulose recalcitrance. Biotechnol. Biofuels. 11, 1–17. https://doi.org/10.1186/s13068-018-1053-8.

Himmel, M.E., Ding, S.Y., Johnson, D.K., Adney, W.S., Nimlos, M.R., Brady, J.W., Foust, T.D., 2007. Biomass recalcitrance: engineering plants and enzymes for biofuels production. Science 315, 804–807. https://doi.org/10.1126/science.1137016.

Hodge, D.B., Karim, M.N., Schell, D.J., McMillan, J.D., 2008. Soluble and insoluble solids contributions to high-solids enzymatic hydrolysis of lignocellulose. Bioresour. Technol. 99, 8940–8948. https://doi.org/10.1016/j.biortech.2008.05.015.

Igarashi, K., Uchihashi, T., Koivula, A., Wada, M., Kimura, S., Okamoto, T., Penttilä, M., Ando, T., Samejima, M., 2011. Traffic jams reduce hydrolytic efficiency of cellulase on cellulose surface. Science 333, 1279–1282. https://doi.org/10.1126/science.1208386.

Ju, X., Engelhard, M., Zhang, X., 2013. An advanced understanding of the specific effects of xylan and surface lignin contents on enzymatic hydrolysis of lignocellulosic biomass. Bioresour. Technol. 132, 137–145. https://doi.org/10.1016/j.biortech.2013.01.049.

Khare, S.K., Pandey, A., Larroche, C., 2015. Current perspectives in enzymatic saccharification of lignocellulosic biomass. Biochem. Eng. J. 102, 38–44. https://doi.org/10.1016/j.bej.2015.02.033.

Koutrouli, M., Karatzas, E., Paez-Espino, D., Pavlopoulos, G.A., 2020. A guide to conquer the biological network era using graph theory. Front. Bioeng. Biotechnol. 8, 34. https://doi.org/10.3389/fbioe.2020.00034.

Ling, Z., Ji, Z., Ding, D., Cao, J., Xu, F., 2016. Microstructural and topochemical characterization of thermally modified poplar (populus cathayaha) cell wall. BioRes. 11, 786–799. https://doi.org/10.15376/biores.11.1.786-799.

Mankar, A.R., Pandey, A., Modak, A., Pant, K., 2021. Pretreatment of lignocellulosic biomass: A review on recent advances. Bioresour. Technol. 334, 125235. https://doi.org/10.1016/j.biortech.2021.125235.

McCann, M.C., Carpita, N.C., 2015. Biomass recalcitrance: a multi-scale, multi-factor, and conversion-specific property. J. Exp. Bot. 66, 4109–4118. https://doi.org/10.1093/jxb/erv267.

Meng, X., Pu, Y., Yoo, C.G., Li, M., Bali, G., Park, D.Y., Gjersing, E., Davis, M.F., Muchero, W., Tuskan, G.A., et al., 2017. An in-depth understanding of biomass recalcitrance using natural poplar variants as the feedstock. ChemSusChem 10, 139–150. https://doi.org/10.1002/cssc.201601303.

Meng, X., Ragauskas, A.J., 2014. Recent advances in understanding the role of cellulose accessibility in enzymatic hydrolysis of lignocellulosic substrates. Curr. Opin. Biotechnol. 27, 150–158. https://doi.org/10.1016/j.copbio.2014.01.014.

Meng, X., Wells, T., Sun, Q., Huang, F., Ragauskas, A., 2015. Insights into the effect of dilute acid, hot water or alkaline pretreatment on the cellulose accessible surface area and the overall porosity of populus. Green Chem. 17, 4239–4246. https://doi.org/10.1039/C5GC00689A.

Mohnen, D., 2008. Pectin structure and biosynthesis. Curr. Opin. Plant. Biol. 11, 266–277. https://doi.org/10.1016/j.pbi.2008.03.006.

Müller, A., Volmer, K., Mishra-Knyrim, M., Polle, A., 2013. Growing poplars for research with and without mycorrhizas. Front. Plant. Sci. 4, 332. https://doi.org/10.3389/fpls.2013.00332.

de Oliveira Santos, V.T., Siqueira, G., Milagres, A.M.F., Ferraz, A., 2018. Role of hemicellulose removal during dilute acid pretreatment on the cellulose accessibility and enzymatic hydrolysis of compositionally diverse sugarcane hybrids. Ind. Crops. Prod. 111, 722–730. https://doi.org/10.1016/j.indcrop.2017.11.053.

Ourselin, S., Roche, A., Prima, S., Ayache, N., 2000. Block matching: A general framework to improve robustness of rigid registration of medical images. In: in: International Conference on Medical Image Computing And Computer-Assisted Intervention. Springer, pp. 557–566. https://doi.org/10.1007/978-3-540-40899-4_57.

Qaseem, M.F., Shaheen, H., Wu, A.M., 2021. Cell wall hemicellulose for sustainable industrial utilization. Renew. Sustain. Energy. Rev. 144, 110996. https://doi.org/10.1016/j.rser.2021.110996.

Santos, R.B., Lee, J.M., Jameel, H., Chang, H.M., Lucia, L.A., 2012. Effects of hardwood structural and chemical characteristics on enzymatic hydrolysis for biofuel production. Bioresour. Technol. 110, 232–238. https://doi.org/10.1016/j.biortech.2012.01.085.

Sheldon, R.A., 2014. Green and sustainable manufacture of chemicals from biomass: state of the art. Green Chem. 16, 950–963. https://doi.org/10.1039/C3GC41935E.

Sorek, N., Yeats, T.H., Szemenyei, H., Youngs, H., Somerville, C.R., 2014. The implications of lignocellulosic biomass chemical composition for the production of advanced biofuels. Bioscience 64, 192–201. https://doi.org/10.1093/biosci/bit037.

Sørlie, M., Keller, M.B., Westh, P., 2023. The interplay between lytic polysaccharide monooxygenases and glycoside hydrolases. Essays. Biochem. 67, 551–559. https://doi.org/10.1042/ebc20220156.

Tao, F., Xiao, B., Qi, Q., Cheng, J., Ji, P., 2022. Digital twin modeling. J. Manuf. Syst. 64, 372–389. https://doi.org/10.1016/j.jmsy.2022.06.015.

Thompson, D.N., Chen, H.C., Grethlein, H.E., 1992. Comparison of pretreatment methods on the basis of available surface area. Bioresour. Technol. 39, 155–163. https://doi.org/10.1016/0960-8524(92)90135-K.

Wang, M., Wang, Y., Liu, J., Yu, H., Liu, P., Yang, Y., Sun, D., Kang, H., Wang, Y., Tang, J., et al., 2024. Integration of advanced biotechnology for green carbon. Green Carbon. https://doi.org/10.1016/j.greenca.2024.02.006.

Willis, L., Refahi, Y., Wightman, R., Landrein, B., Teles, J., Huang, K.C., Meyerowitz, E. M., Jönsson, H., 2016. Cell size and growth regulation in the arabidopsis thaliana apical stem cell niche. Proc. Natl. Acad. Sci. U.S.A. 113, E8238–E8246. https://doi.org/10.1073/pnas.1616768113.

Wolf, S., Wan, Y., McDole, K., 2021. Current approaches to fate mapping and lineage tracing using image data. Development 148, dev198994. https://doi.org/10.1242/dev.198994.

Yang, Q., Zhao, W., Liu, J., He, B., Wang, Y., Yang, T., Zhang, G., He, M., Lu, J., Peng, L., et al., 2020. Quantum dots are conventionally applicable for wide-profiling of wall polymer distribution and destruction in diverse cells of rice. Talanta 208, 120452. https://doi.org/10.1016/j.talanta.2019.120452.

Li, Y., Zhuo, J., Liu, P., Chen, P., Hu, H., Wang, Y., Zhou, S., Tu, Y., Peng, L., Wang, Y., 2018. Distinct wall polymer deconstruction for high biomass digestibility under chemical pretreatment in miscanthus and rice. Carbohyd. Polym. 192, 273–281. doi: 10.1016/j.carbpol.2018.03.013.

Zhang, R., Gao, H., Wang, Y., He, B., Lu, J., Zhu, W., Peng, L., Wang, Y., 2023a. Challenges and perspectives of green-like lignocellulose pretreatments selectable for low-cost biofuels and high-value bioproduction. Bioresource Technology 369, 128315. doi: 10.1016/j.biortech.2022.128315.

Zhang, R., Hu, Z., Peng, H., Liu, P., Wang, Y., Li, J., Lu, J., Wang, Y., Xia, T., Peng, L., 2023b. High density cellulose nanofibril assembly leads to upgraded enzymatic and chemical catalysis of fermentable sugars, cellulose nanocrystals and cellulase production by precisely engineering cellulose synthase complexes. Green Chem. 25, 1096–1106. https://doi.org/10.1039/D2GC03744K.

Zhang, R., Hu, Z., Wang, Y., Hu, H., Li, F., Li, M., Ragauskas, A., Xia, T., Han, H., Tang, J., et al., 2023c. Single-molecular insights into the breakpoint of cellulose nanofibers assembly during saccharification. Nat. Commun. 14, 1100. https://doi.org/10.1038/s41467-023-36856-8.

Zhao, X., Zhang, L., Liu, D., 2012a. Biomass recalcitrance. Part I: the chemical compositions and physical structures affecting the enzymatic hydrolysis of lignocellulose. Biofuel. Bioprod. Biorefin. 6, 465–482. https://doi.org/10.1002/bbb.1331.

Zhao, X., Zhang, L., Liu, D., 2012b. Biomass recalcitrance. Part II: Fundamentals of different pre-treatments to increase the enzymatic digestibility of lignocellulose. Biofuel. Bioprod. Biorefin. 6, 561–579. https://doi.org/10.1002/bbb.1350.

Zoghlami, A., Refahi, Y., Terryn, C., Paës, G., 2019. Multimodal characterization of acid-pretreated poplar reveals spectral and structural parameters strongly correlate with saccharification. Bioresour. Technol. 293, 122015. https://doi.org/10.1016/j.biortech.2019.122015.

Zoghlami, A., Refahi, Y., Terryn, C., Paës, G., 2020. Three-dimensional imaging of plant cell wall deconstruction using fluorescence confocal microscopy. Sustain. Chem. 1, 75–85. https://doi.org/10.3390/suschem1020007.